frontiers | Frontiers in Earth Science

TYPE Original Research
PUBLISHED 28 April 2025
DOI 10.3389/feart.2025.1558551

OPEN ACCESS

EDITED BY
Huan Li,
Central South University, China

REVIEWED BY
Mohamed Faisal,
Central South University, China
Nuerkanati Madayipu,
Chinese Academy of Sciences (CAS), China

*CORRESPONDENCE
Chunying Guo,
guochunying106@163.com
Qiaohui Pi,
2010059@glut.edu.cn

RECEIVED 03 February 2025
ACCEPTED 12 March 2025
PUBLISHED 28 April 2025

CITATION
Luo P, Guo C, Pi Q, Wang N and Liu N (2025) Geological characteristics of neoproterozoic motianling granitic pluton hosting uranium mineralization in North Guangxi, China: Insights from biotite chemistry.
Front. Earth Sci. 13:1558551.
doi: 10.3389/feart.2025.1558551

Geological characteristics of neoproterozoic motianling granitic pluton hosting uranium mineralization in North Guangxi, China: Insights from biotite chemistry

Pailong Luo[1,2], Chunying Guo[1,3,4]*, Qiaohui Pi[5,6]*, Ning Wang[5,6] and Naiyuan Liu[1,3,4]

[1]National Key Laboratory of Uranium Resource Exploration-mining and Nuclear Remote Sensing, Beijing, China, [2]School of Earth Resources, China University of Geosciences, Wuhan, China, [3]China National Nuclear Corporation (CNNC) Beijing Research Institute of Uranium Geology, Beijing, China, [4]China National Nuclear Corporation (CNNC) Key Laboratory of Uranium Resource Exploration and Evaluation Technology, Beijing, China, [5]College of Earth Sciences, Guilin University of Technology, Guilin, China, [6]Guangxi Key Laboratory of Hidden Metallic Ore Deposits Exploration, Guilin University of Technology, Guilin, China

The Motianling pluton represents a characteristic U-bearing granite pluton in South China. Biotite serves as an indicator for the mineralization of metals such as Cu, Sn, and W in granite. Previous studies have extensively investigated the U metallogenic potential of the Motianling pluton, but research on the indicative role of biotite geochemistry in U mineralization remains limited. This study selected biotite from the coarse-grained and medium-grained granites of the Motianling pluton as the research subject. Utilizing optical microscopy, electron probe microanalysis (EPMA), and other techniques, a petrographic and geochemical study was conducted, supplemented by a comprehensive analysis of the geochemical data of biotite from typical U-bearing granites in South China. The analytical results reveal that the biotite in the coarse-grained granite is Fe-biotite (FeO^t: 22.88 to 26.15 wt%, Al_2O_3: 16.62 to 17.76 wt%, MgO: 4.52 to 6.99 wt%, TiO_2: 1.37 to 3.04 wt%), while in the medium-grained granite, it is siderophyllite (FeO^t: 27.96 to 30.02 wt%, Al_2O_3: 17.78 to 18.50 wt%, MgO: 1.41 to 2.01 wt%, TiO_2: 1.43 to 2.03 wt%). Additionally, the biotite in the mediumgrained granite exhibits higher concentrations of Fe and Al but lower levels of Mg and Ti compared to the coarsegrained granite. The geochemical characteristics of biotite indicate that the Motianling granite is S-type granite, characterized by relatively low temperature and low oxygen fugacity (f_{O2}). The geochemical properties of biotite have certain indicative significance for U enrichment. Biotite from the medium-grained granite exhibits higher U concentrations, a lower Th/U ratio, and lower crystallization temperatures and oxygen fugacity relative to the coarsegrained granite, suggesting enhanced U mineralization potential in the medium-grained granite.

KEYWORDS

motianling pluton, biotite, crystallization temperature, oxygen fugacity, uranium enrichment

1 Introduction

South China is a major region for granite-type uranium deposits in China, with the Motianling, Changjiang, Fucheng, Jintan, Douzhashan, and Zhuguangshan plutons examples of typical U-bearing plutons. The uranium deposits in the Motianling pluton are characterized by high-grade (with major deposits have an average grade >0.3%) and large reserves (>1000t U) (Wang et al., 2024a). The study of the Motianling pluton is conducive to mineral exploration in the region and also helps to enrich the theoretical research on granite-type uranium deposits in South China.

Granite is intrinsically linked to the formation of granite-type metal (such as U) deposits (Zhang et al., 2021). Researchers often use methods such as rock geochemistry, geochronology, and isotopic analysis to discuss the genesis of granites and their metal mineralization (Kong et al., 2018; Li et al., 2018; Madayipu et al., 2023; Li et al., 2024). Biotite is a common dark-colored rock-forming mineral in granite that remains stable across a wide range of temperatures and pressures. The chemical composition of biotite is influenced by the magma's composition (Chen X. et al., 2024). Additionally, it is re-equilibration with late-stage subsolidus magma or hydrothermal fluids (Rasmussen and Mortensen, 2013). This makes biotite an ideal mineral for preserving geochemical information regarding the late-stage of magmatic crystallization processes. As a result, biotite's chemical composition is widely employed to infer factors such as rock genesis and the physicochemical conditions of diagenetic processes (Henry et al., 2005; Zhang et al., 2017b; Wan et al., 2022). These physicochemical conditions include temperature and oxygen fugacity, and other parameters, with oxygen fugacity being related to the redox conditions of the environment. The geochemical composition of biotite is often used to discuss its indicative role in granite ore enrichment and mineralization. (Rasmussen and Mortensen, 2013; Maydagán et al., 2016; Azadbakht et al., 2017). Furthermore, extensive arguments have been made for its role in Cu-, Sn-, and W-bearing granites (Sarjoughian et al., 2015; Tang et al., 2019; Yin et al., 2019). However, studies on U-bearing granites are still limited, and whether biotite can serve as an indicator mineral for U-bearing granites requires further investigation.

Previous studies have identified significant geochemical differences in biotite between U-bearing and non-U-bearing granites in South China, highlighting their relevance to U mineralization potential (Chen et al., 2010; Zhang et al., 2011; Chen et al., 2012; Gao et al., 2014; Hu et al., 2014; Zhao K. D. et al., 2016; Zhang et al., 2017a; Zhang et al., 2017b; Zhong et al., 2017; Li et al., 2021; Wan et al., 2022). Biotite in U-bearing granites is typically characterized by lower crystallization temperatures and reduced oxygen fugacity, conditions that promote U enrichment. Despite its significance as a representative U-bearing granite in South China, the Motianling pluton has received limited systematic investigation with regard to the geochemical characteristics of its biotite. The Motianling pluton is generally considered to have formed around 825 to 800 Ma (Zhao et al., 2013; Song et al., 2015; Xu et al., 2019). It is intriguing to explore whether the U mineralization potential differs between the coarse-grained and medium-grained granites, which represent different magmatic facies within the Motianling pluton.

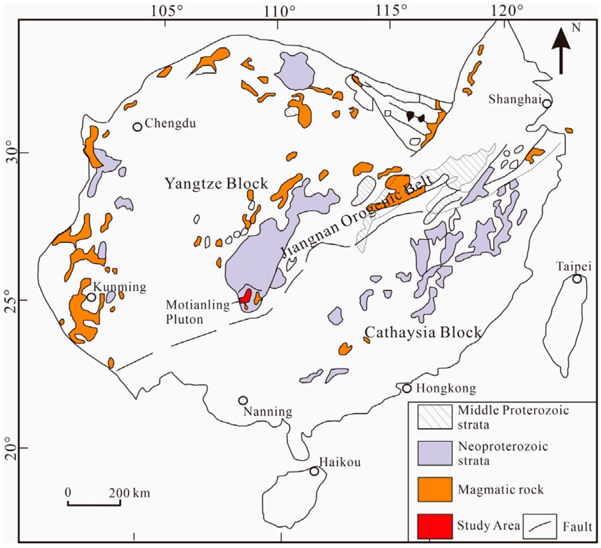

FIGURE 1
Simplified geological map of South China (Wang et al., 2006).

This study focuses on biotite from the coarse-grained and medium-grained granites, which constitute the dominant lithologies of the Motianling pluton. Through comprehensive petrographic observations and geochemical analyses, the study aims to elucidate the prospecting significance of biotite geochemistry for assessing uranium metallogenetic potential within the pluton. Furthermore, by comparing the geochemical characteristics of biotite from the two types of granites, the study investigates variations in their U mineralization potential, thereby providing deeper insights into the metallogenetic mechanisms of the Motianling pluton.

2 Geological setting

The Motianling pluton is situated at the southwest edge of the Jiangnan orogenic belt, at the intersection of the Yangtze Block and the Cathaysia Block (Figure 1). It belongs to the Jiyang domal anticline core within the JiuWanDashan uplift.

The Jiangnan orogenic belt has experienced multiple phases of tectonic orogeny, including the Sibao Orogeny, the Caledonian Orogeny, the Hercynian - Indosinian Orogeny, and the Yanshanian Orogeny - Himalayan Orogeny, among others (Zhang et al., 2013). The study area is strongly influenced by the Caledonian Orogeny and the Yanshanian Orogeny (Qiu et al., 2020).

During the late stage of the Paleproterozoic, the South China region gradually evolved into two continental blocks, the proto-Cathaysia and the proto-Yangtze, with the Paleo-South China Ocean situated between them (Wang et al., 2024b). During the Sibao Orogeny, the Nanyang terrane subducted toward the Yangtze Plate, forming the Jiangnan Proterozoic trench-arc-basin tectonic system (Yao et al., 2019; Chen F. L. et al., 2024). Due to the nearly north-south compression between the Cathaysia Plate and the Yangtze Plate, the Sibao Group strata underwent axial near east-west folding deformation and thrusting, accompanied by a series of metamorphic processes, migmatization, and magmatic activities (Shu et al., 2021). This region developed an island arc accretionary belt, where mantle-derived magma mixed with crustal source materials to form subduction island arc-type hybridized magmatic rocks, while large-scale post-collisional granite intrusions produced plutons such as Motianling (Sanfang) and Yuanbaoshan (Yao et al., 2019). Subsequently, through tectonic evolutions such as the Caledonian and Yanshanian Orogeny, the fold orientations in the region shifted to a NNE-trending structures (Meng et al., 2024).

The basement in the Motianling pluton area consists of Proterozoic formations (including the Sibao Group, Danzhou Group, Nanhua System, and Sinian System) and Early Paleozoic strata (Cambrian, Ordovician, and locally exposed Silurian). The overlying strata, composed predominantly of Devonian sandy conglomerates and carbonate rocks, exhibit discontinuous sedimentary facies (Zhao et al., 2018). Moreover, in some local areas, continental extensional basins have developed, where Cretaceous conglomerates and mudstones were deposited. The Motianling pluton intrudes the Sibao Group and partially penetrates the lower Danzhou Group (Figure 2). The Sibao Group underlies the Danzhou Group, exhibiting angular or parallel unconformity. It is composed of meta-sandstone and mudstone interbedded with intermediate to basic lava, volcanic clastic rocks, and layered or quasi-layered mafic-ultramafic rocks. The Sibao Group outcrops around the Motianling pluton, with a thickness exceeding 5,700 m. The overall attitude of the strata is that they dip away from the pluton, and from bottom to top, they are divided into the Jiuxiao, Wentong, and Yuxi groups (Wang et al., 2024a). The lithology of the Danzhou Group comprises metasandstone and metamudstone, with a small proportion of carbonate rock. It is distributed on the northeastern periphery of the Motianling pluton, near the Cuili area, as well as in the southwestern and southeastern parts, with a thickness ranging from approximately 963–4,780 m, and is divided into the Baizhu, Hetong, and Gongdong groups (Wang et al., 2024a). Magmatic rocks are widely distributed in the area, primarily consisting of intrusive and extrusive rocks from the Middle Proterozoic Sibao orogeny, Neoproterozoic Xuefeng orogeny, and Caledonian orogeny. The area is characterized by developed fault systems, including NE-trending and NW-trending structures. Four major NNE-trending transpression faults, arranged in an east-to-west sequence as follows: the Wuzhishan fault, Gaowu fault, Zishanping fault, and Mamuling fault. The NW-trending faults, which are smaller in scale and later in time, are more numerous and primarily consist of transtensional fault.

The exposed surface area of the pluton in the region spans approximately 955 km^2, presenting a NNE-trending elliptical shape. The pluton is clearly zoned into facies and exhibits gradual zoning. Based on previous studies, the pluton can be divided into the central facies, transitional facies, transitional edge facies, and marginal facies (Xu et al., 2019). The central phase is located at the core of the pluton and is characterized by coarse-grained biotite granite. The transitional phase occurs at the edges of the pluton, adjacent to faults and depressions, and is predominantly composed of mediumgrained biotite granite. The transitional edge phase is distributed between the core and the periphery of the pluton, covering the largest area, and is mainly composed of medium to fine-grained biotite granite. The marginal phase occupies the periphery of the pluton and the peaks of the high mountains, consisting mainly of fine-grained biotite granite. Additionally, in localized areas, gneissic coarse-to medium-coarse-grained porphyritic biotite granite can be observed within the pluton.

More than 20 uranium deposits (mineralization points) have been discovered within the Motianling pluton, primarily distributed in its eastern and southwestern parts, all aligned along the fault trends within the pluton (Figure 2), with the Xincun deposit and the Daliang deposit being the most typical. Within the coarse-grained granite of the Motianling pluton at the Xincun deposit, economic U mineralization bodies are concentrated along the Wuzhishan Fault; in parts of the mining area, fine-grained granite from the Sibao orogeny and banded remnants of biotite-quartz schist are exposed. In total, there are 81 mineralization bodies, ranging from 10 to 306 m in length, with considerable variations in scale, exhibiting vein-like and lenticular forms (Wang et al., 2024a). Its genesis is generally considered to be a hydrothermal uranium deposit, formed against the backdrop of lithospheric extension and thinning during the Cretaceous–Paleogene (Qiu et al., 2018; Wang et al., 2024a). The Daliang deposit is located along the contact zone between the granite body at the southwestern margin of the Motianling pluton and lightly metamorphosed rocks, primarily occurring within the medium-grained biotite granite, with the outcropping strata in the deposit area belonging to the Jiuxiao Group of the Sibao Group. There are over 100 mineralization bodies, each less than 1 m thick, extending 40–80 m along strike and reaching depths of 60–200 m, exhibiting stringer-type, vein-type, and lenticular forms (Qiu et al., 2015). The genesis of the Daliang deposit is analogous to the Xincun deposit, and it is categorized as a hydrothermal uranium deposit (Qiu et al., 2018).

3 Sample characterization and methods of analysis and testing

3.1 Sample characteristics

The samples analyzed in this study were carefully selected from fresh, representative granite specimens collected from the Motianling pluton. The coarse-grained granite sample exhibits a grayish-white, coarse-grained, porphyaceous texture with block-like features (Figures 3A, C). Its primary minerals consist of K-feldspar, plagioclase, quartz, and biotite. In the coarse-grained granite, biotite appears as subhedral to euhedral, sheet-like crystals, with perfect cleavage, positive and moderate relief, ranging in color from yellowish-green to brown, and displaying strong pleochroism. It occurs in symbiotic intergrowth or embayment relationships with muscovite, while hosting accessory minerals such as zircon (Figure 3E). The medium-grained granites exhibit a grayish-white, medium-grained, subhedral granular texture with block-like features (Figures 3B, D). The predominant minerals in these granites consist of K-feldspar, quartz, biotite, muscovite, and a minor amount of tourmaline. Biotite in the medium-grained granites appears subhedral, sheet-like, with perfect cleavage, positive and moderate relief, typically yellowish-brown in color, and showing strong pleochroism. There is no evident inclusion relationship with accessory minerals (Figure 3F).

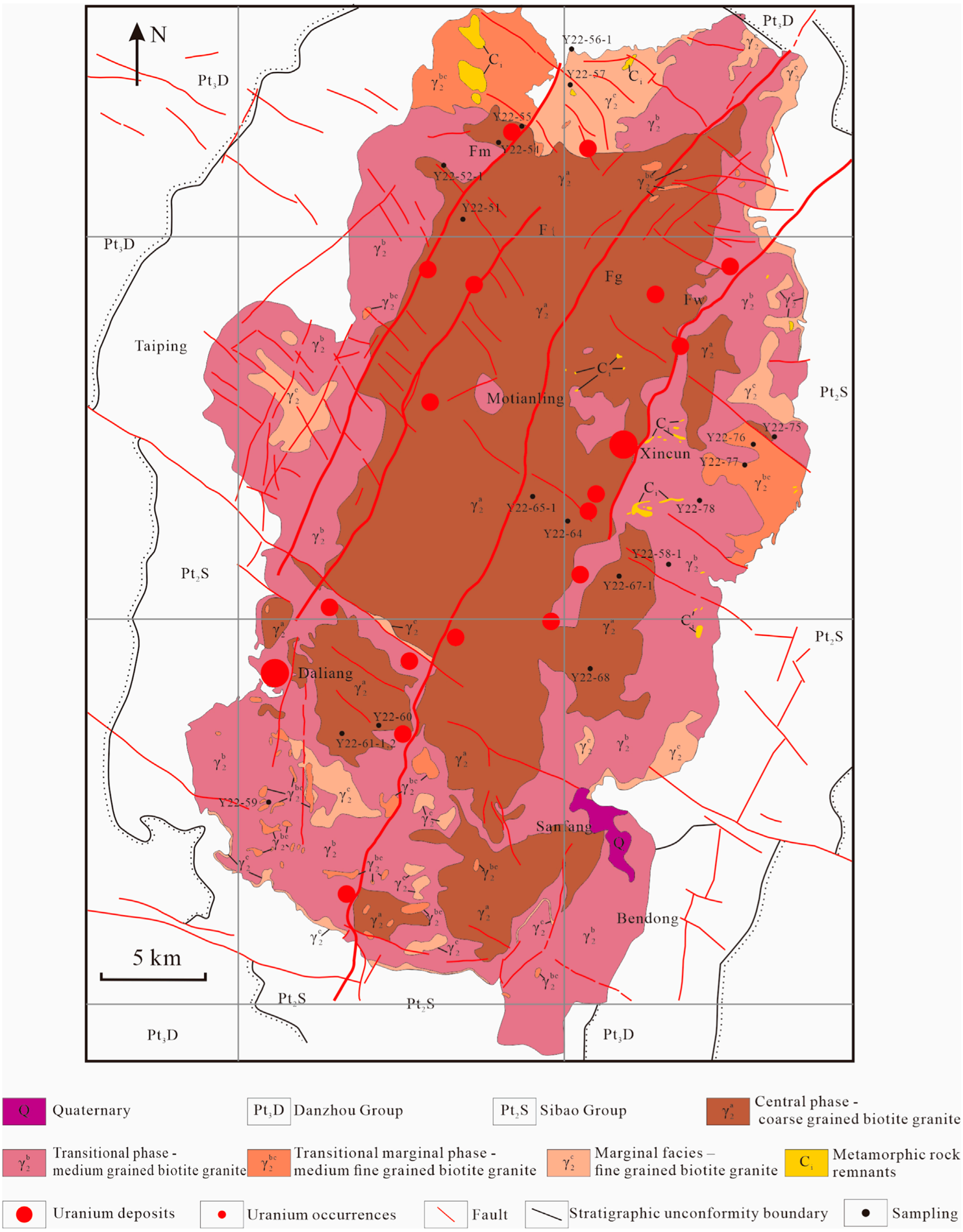

FIGURE 2
Geological map of the Motianling area (Xu et al., 2019).

3.2 Analysis methods

Grind all selected rock samples into probe sections. Following detailed microscopic observation, fresh and unaltered biotite grains were selected for electron microprobe analysis (EMPA). Sample testing was completed by Wuhan Shangpu Analysis Technology Co., Ltd. The instrument used was the JXA-8230 electron microprobe, and the testing conditions were: accelerated voltage of 15kV, probe

FIGURE 3
Field outcrops **(a, b)**, hand specimens **(c, d)**, and microscopic features **(e, f)** of the Motianling granite pluton Bt: Biotite; Q: Quartz; Mus: Muscovite; Pl: plagioclase; Kf: K-feldspar.

current of 1 × 10^{-8} A, counting time of 15s, beam spot diameter of 5 μm. The standard sample adopts the silicate mineral and oxide standard sample from SPI Company in the United States, and the calibration method is the ZAF correction method. The biotite probe data is calculated based on 22 oxygen atoms to calculate their cation numbers and related parameters. Fe^{2+} and Fe^{3+} values were derived using the method of Lin and Peng (1994). The EMPA results and calculated parameters are presented in Tables 1, 2.

4 Results

The study obtained a total of 41 valid data points. Among these, 21 valid data points were obtained from biotite in coarse-grained granite. And 20 valid data points were obtained from biotite in medium-grained granite (Table. 1 and 2). It is evident that the biotite samples from Motianling pluton exhibit elevated levels of Al (16.62–18.5wt%) and Fe (22.88–30.02wt%), with relatively low concentrations of Ti (1.37–3.04wt%) and Mg (1.41–6.99wt%). In coarse-grained granite biotite, compositional ranges are: Fe (22.88–26.15 wt%; average 24.15 wt%), Al (16.62–17.76 wt%; average 17.30 wt%), Mg (4.52–6.99 wt%; average 5.79 wt%), and Ti (1.37–3.04 wt%; average 2.43 wt%). And in mediumgrained granite biotite compositional ranges are: Fe (27.96–30.02 wt%; average 29.02 wt%), Al (17.78–18.50 wt%; average 18.05 wt%), Mg (1.41–2.01 wt%; average 1.53 wt%) and Ti (1.43–2.03 wt%; average 1.82 wt%). Based on biotite compositional variation diagram (Figure 4), the elemental ranges in biotite are generally relatively

TABLE 1 microprobe analyses (EMPA) of biotite from the studied granites.

Number oxides (wt%)	1	2	3	4	5	6	7	8	9	10	11	12	13	14	15	16	17	18	19	20	21
Biotite in the coarse-grained granite																					
TiO2	1.97	2.29	3.03	2.00	2.99	2.09	2.57	2.20	2.66	2.86	2.72	1.80	1.37	2.63	2.74	2.72	2.04	2.90	3.04	2.38	2.05
Al2O3	17.76	17.68	17.39	17.44	17.18	17.06	17.39	17.75	17.70	17.49	16.94	17.49	17.57	17.13	17.16	16.71	17.18	16.62	17.17	17.08	17.36
MnO	0.52	0.41	0.50	0.42	0.47	0.53	0.47	0.53	0.55	0.56	0.48	0.46	0.54	0.46	0.44	0.44	0.51	0.46	0.54	0.54	0.47
MgO	6.44	6.22	5.99	6.46	6.01	4.96	4.64	4.87	4.60	4.52	5.97	6.42	6.99	5.86	5.86	6.05	6.09	5.98	5.57	5.92	6.20
CaO	0.02	0.01	0.01	0.00	0.01	0.01	0.00	0.00	0.02	0.00	0.00	0.00	0.01	0.00	0.00	0.03	0.00	0.00	0.05	0.02	0.02
Na2O	0.07	0.08	0.09	0.11	0.13	0.01	0.05	0.00	0.04	0.04	0.08	0.07	0.07	0.06	0.11	0.07	0.07	0.11	0.10	0.05	0.05
K2O	9.68	9.93	9.77	9.93	9.86	9.87	9.75	9.84	9.48	9.77	9.81	9.95	9.82	9.51	9.71	9.68	9.25	9.65	9.72	10.03	9.67
Cs2O	0.00	0.08	0.00	0.00	0.01	0.11	0.05	0.00	0.00	0.00	0.02	0.00	0.06	0.01	0.12	0.01	0.01	0.10	0.00	0.01	0.00
BaO	0.09	0.13	0.12	0.09	0.10	0.06	0.03	0.03	0.08	0.03	-	-	-	-	-	-	-	-	-	-	-
V2O3	0.01	0.03	0.02	0.03	0.03	0.01	0.06	0.09	0.00	0.07	0.00	0.04	0.09	0.27	0.10	0.18	0.09	0.00	0.00	0.33	0.18
Cr2O3	0.00	0.00	0.03	0.04	0.03	0.03	0.01	0.07	0.05	0.02	0.02	0.08	0.02	0.00	0.03	0.01	0.02	0.02	0.01	0.10	0.09
NiO	0.00	0.01	0.00	0.00	0.00	0.03	0.00	0.00	0.03	0.00	0.00	0.00	0.00	0.00	0.00	0.01	0.00	0.02	0.00	0.00	0.01
ZnO	0.12	0.04	0.07	0.11	0.08	0.00	0.09	0.04	0.04	0.10	0.01	0.00	0.06	0.06	0.07	0.05	0.03	0.10	0.07	0.03	0.03
FeOt	22.88	22.93	24.05	23.41	23.13	25.59	26.15	25.70	25.51	25.84	23.85	23.84	23.26	23.81	23.89	24.44	24.02	23.72	24.25	23.29	23.54
SrO	-	-	-	-	-	-	-	-	-	-	0.00	0.00	0.00	0.10	0.00	0.00	0.06	0.06	0.00	0.01	0.03
F	-	-	-	-	-	-	-	-	-	-	0.00	0.03	0.00	0.00	0.00	0.00	0.00	0.01	0.07	0.02	0.00
Cl	-	-	-	-	-	-	-	-	-	-	0.03	0.01	0.02	0.03	0.01	0.00	0.00	0.01	0.00	0.01	0.01
Total	94.88	96.28	96.72	96.61	96.05	95.81	96.48	96.16	96.40	96.70	95.08	94.93	95.40	94.47	94.90	94.99	94.15	94.12	95.53	94.75	94.52
Cations calculated based on 22 oxygen atoms (anhydrous)																					
Si	5.49	5.56	5.46	5.58	5.53	5.53	5.46	5.45	5.49	5.46	5.48	5.44	5.51	5.44	5.43	5.43	5.47	5.43	5.43	5.49	5.46
AlIV	2.51	2.44	2.54	2.42	2.47	2.47	2.54	2.55	2.51	2.54	2.52	2.56	2.49	2.56	2.57	2.57	2.53	2.57	2.57	2.51	2.54
AlVI	0.73	0.74	0.59	0.71	0.63	0.66	0.64	0.70	0.70	0.64	0.59	0.67	0.71	0.62	0.60	0.52	0.66	0.53	0.57	0.65	0.67

(Continued on the following page)

TABLE 1 (*Continued*) Electron microprobe analyses (EMPA) of biotite from the studied granites.

Number oxides (wt%)	1	2	3	4	5	6	7	8	9	10	11	12	13	14	15	16	17	18	19	20	21
Ti	0.23	0.26	0.35	0.23	0.35	0.25	0.30	0.26	0.31	0.33	0.32	0.21	0.16	0.31	0.32	0.32	0.24	0.34	0.36	0.28	0.24
Fe3+	0.39	0.42	0.42	0.40	0.42	0.41	0.42	0.41	0.46	0.44	0.40	0.34	0.35	0.41	0.39	0.38	0.40	0.39	0.41	0.38	0.38
Fe2+	2.58	2.51	2.66	2.58	2.54	2.93	2.97	2.93	2.82	2.89	2.71	2.78	2.66	2.73	2.73	2.83	2.75	2.75	2.74	2.68	2.71
Mn	0.07	0.05	0.06	0.05	0.06	0.07	0.06	0.07	0.07	0.07	0.06	0.06	0.07	0.06	0.06	0.06	0.07	0.06	0.07	0.07	0.06
Mg	1.49	1.42	1.37	1.47	1.37	1.15	1.07	1.13	1.06	1.04	1.39	1.50	1.61	1.37	1.37	1.42	1.43	1.41	1.29	1.39	1.45
Ca	0.00	0.00	0.00	0.00	0.00	0.00	0.00	0.00	0.00	0.00	0.00	0.00	0.00	0.00	0.00	0.01	0.00	0.00	0.01	0.00	0.00
Na	0.02	0.03	0.03	0.03	0.04	0.00	0.02	0.00	0.01	0.01	0.03	0.02	0.02	0.02	0.03	0.02	0.02	0.03	0.03	0.01	0.02
K	1.92	1.93	1.91	1.93	1.93	1.96	1.93	1.95	1.86	1.92	1.95	1.99	1.94	1.91	1.94	1.94	1.86	1.95	1.93	2.01	1.94
Cl	0.00	0.00	0.00	0.00	0.00	0.00	0.00	0.00	0.00	0.00	0.00	0.01	0.00	0.00	0.00	0.00	0.00	0.00	0.02	0.01	0.00
F	0.00	0.00	0.00	0.00	0.00	0.00	0.00	0.00	0.00	0.00	0.02	0.01	0.01	0.01	0.00	0.00	0.00	0.01	0.00	0.01	0.00
Total	15.43	15.36	15.39	15.41	15.35	15.44	15.41	15.44	15.30	15.36	15.45	15.58	15.54	15.43	15.45	15.49	15.43	15.48	15.42	15.48	15.48

Number oxides (wt%)	1	2	3	4	5	6	7	8	9	10	11	12	13	14	15	16	17	18	19	20
Biotite in the coarse-grained granite																				
SiO2	34.08	33.07	33.84	33.79	33.42	34.27	33.36	33.75	33.67	34.05	34.43	34.36	33.93	33.91	33.98	34.12	33.93	33.80	34.26	33.78
TiO2	1.56	1.84	1.93	1.43	1.47	1.96	1.77	1.88	1.85	2.00	1.75	1.62	1.96	1.77	2.03	1.87	1.91	1.91	1.89	1.94
Al2O3	18.50	17.78	17.96	18.15	18.34	18.06	17.98	17.98	17.95	18.16	18.32	18.14	18.02	18.11	17.82	18.01	17.86	17.78	18.02	18.02
MnO	0.61	0.67	0.63	0.64	0.60	0.58	0.67	0.68	0.69	0.55	0.57	0.66	0.57	0.66	0.72	0.77	0.69	0.57	0.57	0.65
MgO	1.47	1.61	1.52	1.42	2.01	1.52	1.58	1.42	1.55	1.49	1.46	1.53	1.41	1.45	1.47	1.56	1.51	1.58	1.52	1.59
CaO	0.00	0.00	0.02	0.00	0.03	0.06	0.02	0.03	0.02	0.00	0.00	0.00	0.06	0.01	0.04	0.01	0.02	0.03	0.01	0.02
Na2O	0.03	0.01	0.04	0.02	0.04	0.05	0.03	0.08	0.04	0.08	0.04	0.01	0.05	0.03	0.09	0.06	0.04	0.00	0.07	0.08
K2O	9.54	8.94	9.37	9.52	8.77	9.18	9.51	9.33	9.17	9.60	9.47	9.44	9.36	9.48	9.60	9.29	9.64	9.53	9.50	9.21
Cs2O	0.04	0.02	0.03	0.01	0.07	0.05	0.07	0.12	0.00	0.01	0.12	0.15	0.03	0.00	0.09	0.13	0.17	0.10	0.13	0.05

(Continued on the following page)

TABLE 1 (*Continued*) Electron microprobe analyses (EMPA) of biotite from the studied granites.

Number oxides (wt%)	1	2	3	4	5	6	7	8	9	10	11	12	13	14	15	16	17	18	19	20
BaO																				
V2O3	0.00	0.18	0.00	0.00	0.23	0.18	0.00	0.11	0.00	0.09	0.00	0.00	0.13	0.00	0.00	0.21	0.00	0.00	0.18	0.08
Cr2O3	0.04	0.04	0.04	0.01	0.03	0.01	0.06	0.00	0.04	0.04	0.03	0.00	0.03	0.00	0.02	0.04	0.00	0.03	0.03	0.00
NiO	0.00	0.00	0.02	0.00	0.00	0.01	0.02	0.10	0.00	0.03	0.00	0.00	0.06	0.00	0.00	0.05	0.00	0.00	0.00	0.01
ZnO	0.14	0.13	0.12	0.18	0.11	0.07	0.16	0.23	0.11	0.12	0.12	0.10	0.00	0.11	0.06	0.13	0.10	0.15	0.13	0.02
FeOt	28.63	30.02	29.34	28.91	28.89	27.96	29.70	28.33	28.82	28.41	29.21	28.93	28.91	29.29	29.24	29.02	29.11	28.95	29.19	29.44
SrO	0.03	0.00	0.00	0.02	0.08	0.00	0.03	0.01	0.00	0.00	0.00	0.01	0.04	0.02	0.00	0.00	0.00	0.00	0.00	0.11
F	0.14	0.01	0.00	0.06	0.15	0.06	0.00	0.00	0.03	0.08	0.00	0.00	0.19	0.00	0.04	0.00	0.13	0.00	0.14	0.04
Cl	0.04	0.04	0.03	0.04	0.04	0.04	0.05	0.04	0.05	0.04	0.04	0.07	0.05	0.03	0.03	0.06	0.06	0.03	0.06	0.04
Total	94.78	94.34	94.89	94.17	94.21	94.02	94.98	94.08	93.97	94.71	95.54	95.00	94.71	94.86	95.21	95.31	95.10	94.46	95.62	95.03
Cations calculated based on 22 oxygen atoms (anhydrous)																				
Si	5.48	5.39	5.45	5.48	5.42	5.53	5.40	5.48	5.46	5.48	5.49	5.51	5.47	5.46	5.46	5.48	5.46	5.47	5.48	5.44
AlIV	2.52	2.61	2.55	2.52	2.58	2.47	2.60	2.52	2.54	2.52	2.51	2.49	2.53	2.54	2.54	2.52	2.54	2.53	2.52	2.56
AlVI	0.98	0.81	0.86	0.95	0.92	0.96	0.84	0.93	0.89	0.92	0.94	0.94	0.89	0.90	0.84	0.89	0.85	0.86	0.88	0.85
Ti	0.19	0.23	0.23	0.17	0.18	0.24	0.22	0.23	0.23	0.24	0.21	0.19	0.24	0.21	0.25	0.23	0.23	0.23	0.23	0.23
Fe3+	0.27	0.26	0.27	0.26	0.27	0.29	0.25	0.27	0.27	0.27	0.28	0.27	0.27	0.27	0.26	0.27	0.26	0.27	0.27	0.27
Fe2+	3.58	3.83	3.69	3.66	3.64	3.48	3.78	3.58	3.64	3.55	3.62	3.61	3.62	3.68	3.67	3.62	3.66	3.65	3.64	3.69
Mn	0.08	0.09	0.09	0.09	0.08	0.08	0.09	0.09	0.09	0.08	0.08	0.09	0.08	0.09	0.10	0.10	0.09	0.08	0.08	0.09
Mg	0.35	0.39	0.36	0.34	0.49	0.36	0.38	0.34	0.38	0.36	0.35	0.37	0.34	0.35	0.35	0.37	0.36	0.38	0.36	0.38
Ca	0.00	0.00	0.00	0.00	0.01	0.01	0.00	0.00	0.00	0.00	0.00	0.00	0.01	0.00	0.01	0.00	0.00	0.01	0.00	0.00

(Continued on the following page)

TABLE 1 (*Continued*) Electron microprobe analyses (EMPA) of biotite from the studied granites.

Number oxides (wt%)	1	2	3	4	5	6	7	8	9	10	11	12	13	14	15	16	17	18	19	20
Na	0.01	0.00	0.01	0.01	0.01	0.02	0.01	0.03	0.01	0.02	0.01	0.00	0.01	0.01	0.03	0.02	0.01	0.00	0.02	0.02
K	1.96	1.86	1.93	1.97	1.81	1.89	1.96	1.93	1.90	1.97	1.93	1.93	1.92	1.95	1.97	1.90	1.98	1.97	1.94	1.89
Cl	0.04	0.00	0.00	0.02	0.04	0.02	0.00	0.00	0.01	0.02	0.00	0.00	0.05	0.00	0.01	0.00	0.03	0.00	0.04	0.01
F	0.02	0.02	0.02	0.02	0.02	0.02	0.02	0.02	0.02	0.02	0.02	0.03	0.02	0.02	0.02	0.03	0.03	0.01	0.03	0.02
Total	15.47	15.49	15.46	15.49	15.47	15.36	15.55	15.43	15.44	15.45	15.43	15.44	15.47	15.47	15.49	15.44	15.52	15.47	15.48	15.47

"-" represents undetected.

concentrated; only the Ti, Mg, and Fe content ranges in biotite from coarse-grained granite are relatively wide, while in mediumgrained granite, only the Fe content range is relatively wide. The Ti, Al, Mg, K, and Fe contents in biotite differ significantly between the two types of granite. Medium-grained granite biotite is enriched in Fe and Al, but poor in Ti and Mg compared to coarse-grained granite biotite. According to the biotite classification diagram (Foster, 1960). The biotite in coarse-grained granite primarily falls within the domain of Fe-biotite, while the biotite in medium-grained granite predominantly falls within the domain of siderophyllite (Figure 5). Significant compositional divergence in biotite is found between the two granite lithologies.

5 Discussion

5.1 Biotite genesis types

Based on genetic classification, biotite can be categorized into magmatic biotite, hydrothermal metasomatic biotite (recrystallized biotite), and hydrothermal neobiotite (Jacobs and Parry, 1976; Tang et al., 2017; Wan et al., 2022). There are significant differences in petrographic and mineral chemistry between magmatic biotite and hydrothermal biotite. In terms of petrography, the biotite found in the granite of the Motianling pluton typically occurs in sheet-like euhedral to Subhedral form, exhibiting serrated and fractured features, and often enclosing early accessory minerals (Figures 3E, F). This biotite is classified as magmatic biotite (Selby and Nesbitt, 2000; Tang et al., 2017). Magmatic biotite has a moderate Ti ion number ($0.20<Ti < 0.55$) in terms of mineral chemical properties, with X_{Mg} values ranging from 0.30 to 0.55 (Liu et al., 2010). Other studies indicate that the Mg/Fe ratio of magmatic biotite is less than 1.0, whereas that of altered biotite is more than 1.5 and Fe^{3+}/Fe^{2+} is less than 0.3 (Beane, 1974). The Ti ion number of biotite in the coarse-grained granite of Motianling ranges from 0.16 to 0.36 (average 0.28), with X_{Mg} values ranging from 0.24 to 0.35 (average 0.30), and Mg/Fe values ranging from 0.31 to 0.54 (average 0.43). For the medium-grained granite, the Ti ion number of biotite ranges from 0.17 to 0.25 (average 0.22), with X_{Mg} values ranging from 0.08 to 0.11 (average 0.09), and Mg/Fe values ranging from 0.09 to 0.12 (average 0.0.9). Besides, the $Fe^{2+}/(Fe^{2+}+Mg^{2+})$ ratio in biotite from coarse-grained granite ranges from 0.62 to 0.74; in medium-grained granite, it ranges from 0.88 to 0.91. The narrow range of these ratios suggests that these biotites are less affected by later hydrothermal events (Stone, 2000). And they are similar to the characteristics of biotite in typical uranium-bearing granites in South China (>0.65) (Chen et al., 2012; Zhang et al., 2017a). Based on the petrographic and mineral chemical analysis, the biotite in both coarse-grained and medium-grained granites is considered magmatic biotite.

5.2 Comparison of biotite types and biotite in granite of different origins

Geochemical characteristics of biotite (such as Mg, Fe and Al content) can provide important information for the material source and genesis of granite magma (Abdel and Abdel, 1994;

10.3389/feart.2025.1558551

TABLE 2 Relevant parameters based on biotite test data and cation number calculation.

Number	1	2	3	4	5	6	7	8	9	10	11	12	13	14	15	16	17	18	19	20	21
Biotite in the coarse-grained granite																					
Fe_2O_3(cal)	3.37	3.64	3.62	3.52	3.67	3.49	3.63	3.49	3.97	3.81	3.40	2.87	3.01	3.43	3.35	3.22	3.42	3.25	3.52	3.23	3.24
FeO(cal)	19.85	19.66	20.79	20.24	19.83	22.44	22.88	22.56	21.93	22.41	20.79	21.26	20.55	20.72	20.87	21.54	20.94	20.79	21.08	20.38	20.62
Fe^{2+}+Mn	2.64	2.56	2.73	2.64	2.60	3.00	3.03	3.00	2.90	2.97	2.77	2.84	2.73	2.79	2.79	2.89	2.82	2.81	2.81	2.75	2.77
Al^{VI}+Fe^{3+}+Ti	1.36	1.42	1.36	1.34	1.40	1.32	1.36	1.36	1.47	1.42	1.30	1.22	1.22	1.33	1.32	1.22	1.30	1.26	1.34	1.31	1.30
XMg	0.33	0.33	0.31	0.33	0.32	0.26	0.24	0.25	0.24	0.24	0.31	0.32	0.35	0.30	0.30	0.31	0.31	0.31	0.29	0.31	0.32
P (kbar)	3.31	3.11	2.97	2.96	2.88	2.97	3.10	3.32	3.21	3.11	2.89	3.25	3.19	3.10	3.07	2.84	3.12	2.86	2.99	3.04	3.20
H (km)	12.53	11.75	11.23	11.20	10.89	11.23	11.73	12.55	12.12	11.75	10.93	12.27	12.05	11.71	11.60	10.72	11.78	10.80	11.31	11.50	12.08
T (°C)	586	611	659	585	658	592	629	601	634	647	644	568	501	640	646	645	594	657	661	622	595
log$f$O2	−17.43	−16.99	−16.49	−17.44	−16.38	−17.66	−17.17	−17.54	−16.97	−16.87	−16.73	−17.90	−18.91	−16.81	−16.73	−16.83	−17.48	−16.59	−16.54	−17.00	−17.42
MF	0.33	0.32	0.30	0.33	0.31	0.25	0.24	0.25	0.24	0.23	0.30	0.32	0.34	0.30	0.30	0.30	0.31	0.31	0.29	0.31	0.32
$FeO^t/(FeO^t + MgO)$	0.78	0.79	0.80	0.79	0.80	0.84	0.85	0.84	0.85	0.85	0.80	0.79	0.77	0.80	0.81	0.80	0.80	0.80	0.82	0.80	0.79
Mg/Fe	0.50	0.48	0.44	0.49	0.46	0.35	0.32	0.34	0.32	0.31	0.45	0.48	0.54	0.44	0.44	0.44	0.45	0.45	0.41	0.45	0.47

Number	1	2	3	4	5	6	7	8	9	10	11	12	13	14	15	16	17	18	19	20
Biotite in the medium-grained granite																				
FeO(cal)	26.63	28.08	27.35	26.98	26.89	25.82	27.88	26.32	26.80	26.40	27.15	26.88	26.87	27.32	27.30	26.98	27.18	26.99	27.17	27.44
Fe_2O_3(cal)	2.22	2.16	2.21	2.15	2.22	2.37	2.02	2.24	2.25	2.23	2.29	2.27	2.27	2.19	2.15	2.27	2.14	2.18	2.24	2.22
FeO(cal)	26.63	28.08	27.35	26.98	26.89	25.82	27.88	26.32	26.80	26.40	27.15	26.88	26.87	27.32	27.30	26.98	27.18	26.99	27.17	27.44
Fe^{2+}+Mn	3.66	3.92	3.77	3.75	3.73	3.56	3.87	3.67	3.73	3.63	3.70	3.70	3.70	3.77	3.77	3.73	3.75	3.73	3.71	3.78
Al^{VI}+Fe^{3+}+Ti	1.44	1.30	1.36	1.39	1.37	1.48	1.30	1.43	1.39	1.43	1.42	1.41	1.40	1.38	1.34	1.39	1.35	1.36	1.38	1.36
XMg	0.08	0.09	0.08	0.08	0.11	0.09	0.09	0.08	0.09	0.09	0.08	0.09	0.08	0.08	0.08	0.09	0.08	0.09	0.08	0.09

(Continued on the following page)

TABLE 2 (*Continued*) Relevant parameters based on biotite test data and cation number calculation.

Number	1	2	3	4	5	6	7	8	9	10	11	12	13	14	15	16	17	18	19	20
P (kbar)	4.08	3.82	3.80	3.99	4.08	3.87	3.87	3.90	3.87	3.90	3.91	3.86	3.84	3.88	3.70	3.80	3.74	3.75	3.77	3.83
H (km)	15.44	14.43	14.36	15.06	15.42	14.62	14.63	14.74	14.61	14.75	14.77	14.59	14.51	14.68	13.97	14.36	14.14	14.16	14.24	14.46
T (°C)	526	569	577	507	514	580	558	573	569	584	552	535	580	557	586	569	574	576	571	577
log*f*O2	−19.24	−18.71	−18.50	−19.63	−19.50	−18.30	−18.85	−18.47	−18.59	−18.29	−18.84	−19.11	−18.40	−18.80	−18.34	−18.57	−18.52	−18.49	−18.56	−18.50
MF	0.08	0.09	0.08	0.08	0.11	0.09	0.08	0.08	0.09	0.08	0.08	0.08	0.08	0.08	0.08	0.09	0.08	0.09	0.08	0.09
$FeO^t/(FeO^t + MgO)$	0.95	0.95	0.95	0.95	0.94	0.95	0.95	0.95	0.95	0.95	0.95	0.95	0.95	0.95	0.95	0.95	0.95	0.95	0.95	0.95
Mg/Fe	0.09	0.10	0.09	0.09	0.12	0.10	0.10	0.09	0.10	0.09	0.09	0.09	0.09	0.09	0.09	0.10	0.09	0.10	0.09	0.10

The calculation method for Fe_2O_3(cal)、FeO(cal) is calculated according to equations in Lin and Peng (1994); Al^T is the total number of Al cations calculated based on 22 oxygen atoms in biotite; X_{Mg}, Mg/(Mg + Fe); and The $\log_{fO2}$ calculation method comes from Burkhard (1991); 5: MF, Mg/(Mg + Fe^{2+}+Fe^{3+}+Mn).

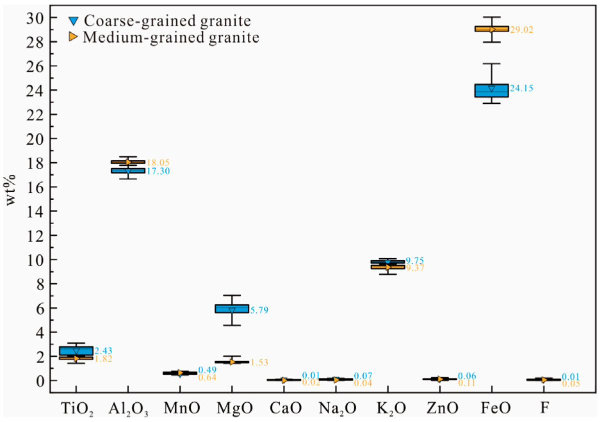

FIGURE 4
Biotite element characteristic diagram The whisker lines in the diagram represent the range from the maximum to the minimum values, and the numbers indicate the mean values.

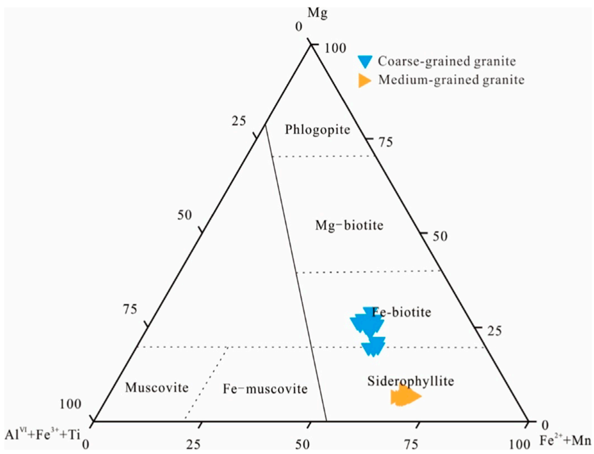

FIGURE 5
Biotite classification diagram (Foster, 1960).

Wan et al., 2022). Research has indicated that the mafic components of biotite are closely related to the material source of granite magma. The rock type diagram (Figure 6) can be utilized to estimate the type of granite, demonstrating that data points for both coarse-grained and mediumgrained granite biotite are situated within the peraluminous suites area (Abdel and Abdel, 1994). This indicates that the Motianling granite belongs to the peraluminous granite category. Research has shown that the geological environment of biotite origin can be determined by the source identification diagram (Figure 7) (Zhou, 1986). The diagram indicates that the biotite from coarse-grained granite and medium-grained granite is located in the crust source region. The iron magnesium index (MF) of biotite, MF = Mg/(Mg + Fe^{2+}+Fe^{3+}+Mn), can be used to distinguish granite genesis (Zhao et al., 1983). In the transformation type granites (S-type granites), the MF of biotite is less than 0.38. In the coarse-grained granite, the MF of biotite ranges from 0.23 to 0.34 (average 0.30). In the medium-grained granite, the MF

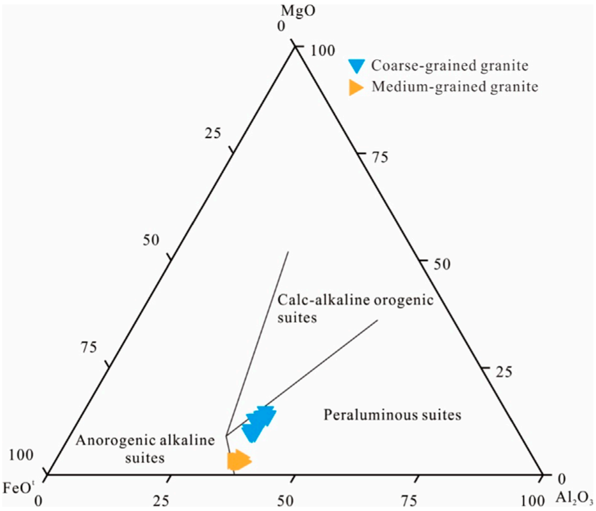

FIGURE 6
Rock type diagram (Abdel and Abdel, 1994).

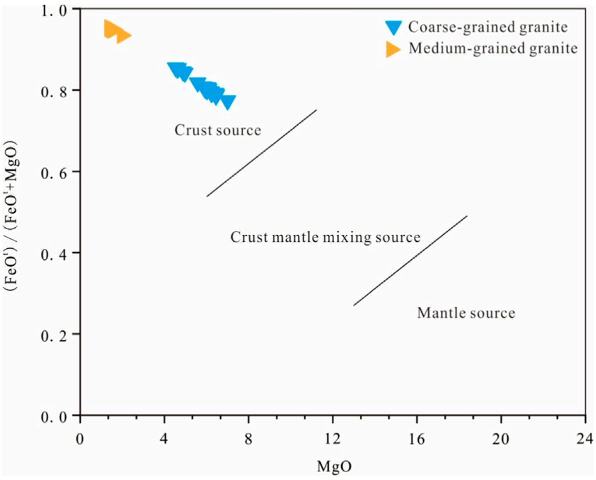

FIGURE 7
Source identification diagram (Zhou, 1986).

of biotite ranges from 0.08 to 0.11 (average 0.08). This suggests that the source rocks of the Motianling granite is pelitic rocks. During the crystallization of coarse-grained granite, the magma incorporated some Mg-rich material, implying that the source region may contain some sandstone. The medium-grained granite is richer in Fe, indicating more extensive magma evolution. In the modified granites (S-type granites), biotite exhibits low magnesium and high iron, aluminum, and lithium content. The types of biotite include Fe-biotite, siderophyllite, and Fe-muscovite (Liu, 1984). The biotite in the Motianling granite is also characterized by high Fe content and low Mg content. The predominant types of biotite are Fe-biotite and siderophyllite. All these characteristics also confirm that the Motianling granite belongs to S-type granite.

Based on the major and trace element characteristics of granite from the Motianling pluton, researchers have concluded in recent years that it is S-type granite (Xu et al., 2019; Wang et al., 2020). Furthermore, studies that combine zircon geochronology with trace element data have discussed the tectonic evolution of the Motianling pluton and concluded that it formed during the late collisional phase of the orogenic process (Wang et al., 2006; Song et al., 2015). These studies indicate that, Motianling pluton genesis should be attributed to the upwelling of deep mantle material during the late collision stage between the Cathaysia-Yangtze Block, resulting in partial melting of the overlying lithosphere and continental crust. The characteristics of biotite reflected in this study are consistent with the rock genesis identified in previous research.

5.3 Physical and chemical conditions of magma crystallization reflected by biotite

5.3.1 Temperature

Henry et al. (2005) found a linear relationship between Ti content, temperature, and X_{Mg}, and summarized the empirical formula for temperature: $t = [\ln(Ti)\text{-}a\text{-}c\,(X_{Mg})^3/b]^{0.333}$

Where t is temperature (°C), Ti is the number of atoms after the number of cations calculated in 22 O atoms, $X_{Mg} = Mg/(Mg + Fe)$, $a = -2.3594$, $b = 4.6482 \times 10^{-9}$, $c = -1.7283$. The application ranges of X_{Mg}, Ti, and t are 0.27–1.000, 0.040 to 0.600, and 400°C–800°C, respectively. Although Henry suggested that this formula be used for metamorphic rocks, in recent years, several studies have applied it to igneous rocks (such as granite) (Tang et al., 2019; Azadbakht et al., 2020; Zhang et al., 2021; Taghavi et al., 2022; Zhang et al., 2023).

In the coarse-grained granite, the X_{Mg} value of biotite ranges from 0.24 to 0.35 (average 0.30), while the Ti content ranges from 0.16 to 0.36 (average 0.28). In the medium-grained granite, the X_{Mg} value of biotite ranges from 0.08 to 0.11 (average 0.09), and the Ti content ranges from 0.17 to 0.25 (average 0.22). The results obtained from the coarse-grained granite meet the prerequisites for the application of this formula, whereas those from the medium-grained granite can only serve as a reference. According to the calculations, the crystallization temperature of the coarse-grained granite ranges from 501°C to 661°C (average 618°C), while that of the medium-grained granite ranges from 507°C to 586°C (average 562°C). These results are consistent with temperature estimates from the crystallization temperature diagram (Figure 8), suggesting that the overall crystallization temperature of the Motianling granite is relatively low, with the coarse-grained granite exhibiting slightly elevated crystallization temperatures compared to the medium-grained granite.

5.3.2 Pressure

Based on the good linear relationship between granite biotite Al^T and diagenetic pressure, Uchida proposed a formula for calculating pressure using biotite Al^T (Uchida et al., 2007):

$$P\,(\text{kbar}) = 3.03 \times A1^T - 6.53\,(\pm 3.33)$$

Wherein Al^T is the total number of Al cations calculated based on 22 oxygen atoms of biotite.

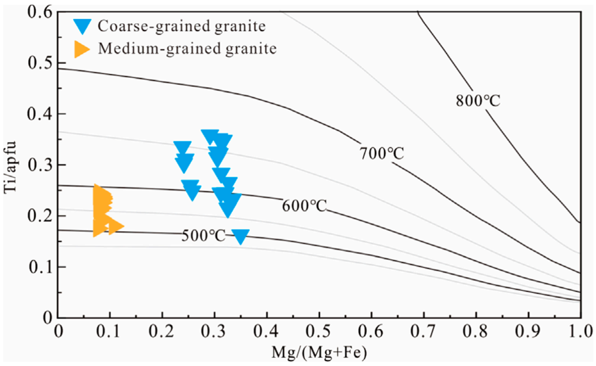

FIGURE 8
Crystallization temperature estimation diagram (Henry et al., 2005).

According to the formula, the solidification pressure range for the coarse-grained granite is estimated at 2.84–3.32 kbar (average 3.07 kbar). For the medium-grained granite, the solidification pressure range is estimated at 3.70–4.08 kbar (average 3.86 kbar). The diagenetic pressure of the medium-grained granite in the Motianling pluton is greater than that of the coarse-grained granite.

5.3.3 Oxygen fugacity

During the crystallization process of magmatic biotite, biotite formed in high oxygen fugacity environments tends to have a higher Mg content, while biotite formed in low oxygen fugacity environments tends to have a higher Fe content (Henry et al., 2005). The six-coordinated aluminum Al^{VI} of biotite is an indicator of the oxygen fugacity of magma crystallization, and a low Al^{VI} value suggests a high oxygen fugacity in the rock formation environment (Buddington and Lindsley, 1964). The biotite in the coarse-grained and medium-grained granites exhibit high Fe and low Mg characteristics (Table 2). Considering that the coarse-grained granite of biotite exhibits an Al^{VI} (apfu) range from 0.59 to 0.74 (average 0.68), and the medium-grained granite of biotite exhibits an Al^{VI} (apfu) range from 0.75 to 0.89 (average 0.82), it can be inferred that the oxygen fugacity of the Motianling granite was generally low, but that the oxygen fugacity of the coarse-grained granite was higher than that of the medium-grained granite.

Previous studies have shown that Fe^{3+}, Fe^{2+}, and Mg^{2+} values in biotite coexisting with magnetite and potassium feldspar can be used to estimate oxygen fugacity during crystallization (David and Hans, 1965). According to the biotite oxygen fugacity estimation diagram (Figure 9), all biotite samples from the coarse-grained granite fall near the NNO (Ni-NiO) buffer line, while all biotite samples from the medium-grained granite fall near the FMQ (Fe_2SiO_4-SiO_2-Fe_3O_4) buffer line.

Based on the empirical formula for oxygen fugacity established by previous studies, it is possible to quantify the oxygen fugacity of plutons (Burkhard, 1991):

$$-1/2 \log f_{O2} = 4819/T + 6.69 + 3\log X_{Fe2+} - \log f_{H2O}$$
$$-\log a_{san} - \log a_{mt} - 0.011(P-1)/T,$$

Among the variables, T represents temperature in Kelvin, P is measured in bar, a_{san} denotes the activity of potassium feldspar,

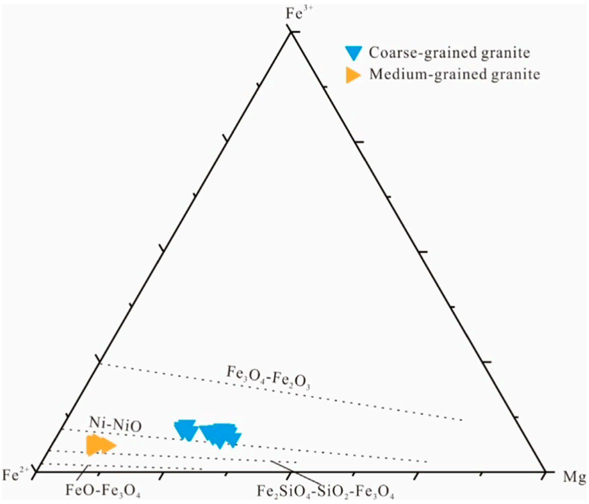

FIGURE 9
Biotite oxygen fugacity estimation diagram (David and Hans, 1965).

and amt indicates the activity of magnetite. The equation $\log f_{H2O} = 2.45 + 0.001T$ (P = 4.5 kbar) is also used, where $\log f_{H2O}$ is the logarithm of the fugacity of water. As ilmenite-series granite lacks magnetite minerals, a_{mt} is assumed to be 0.2 (Czamanske et al., 1981). Whenever the temperature exceeds 600 °C, a_{san} must be at least 0.75. By applying the above formula, the oxygen fugacity of the coarse-grained granite ranges from −18.91 to −16.38 (average −17.14). Conversely, the oxygen fugacity of the medium-grained granite ranges from −19.63 to −18.29 (average −18.71). These results are consistent with the biotite six-fold coordination aluminum (Al^{VI}) properties and the biotite oxygen fugacity estimation diagram results, indicating that the oxygen fugacity of the Motianling granite magma is generally low and that the oxygen fugacity of the coarse-grained granite is higher than that of the medium-grained granite.

5.4 Comparison of biotite temperature and pressure, oxygen fugacity, and uranium producing granite

Uranium-producing granites in South China are mainly distributed in the Jintan pluton, Yangtze River pluton, Douzhashan pluton, Zhuguangshan pluton, Longyuanba pluton, Fucheng pluton, Dafushan pluton, and Xiazhuang pluton.

(Chen et al., 2010; Zhang et al., 2011; Gao et al., 2014; Hu et al., 2014; Gao, 2016; Zhao Y. D. et al., 2016; Zhang et al., 2017b; Zhong et al., 2017; Tao et al., 2020; Pei, 2022). Previous studies on biotite in South China U-bearing granites have shown that the biotite in these granites is enriched in Fe, Al, and F, and that its types include Fe-biotite and siderophyllite, with the latter being predominant. The biotite characteristics of the Motianling pluton are consistent with those of biotite in South China U-bearing granites. The biotite in U-bearing granites in South China (Table 3) has revealed that the crystallization temperature ranges from 499°C to 722°C, the pressure ranges from 0.84 to 5.91 kbar, and the oxygen fugacity ranges between −19.67 and −16.58. It is evident

TABLE 3 Characteristics of temperature, pressure, and oxygen fugacity of uranium producing granite in South China.

Granitic mass	P (kbar)	T (°C)	$\log_{fO2}$
Coarse-grained granite of the Motianling rock mass	2.84~3.32	501~661	−18.91~-16.38
Medium-grained granite of the Motianling rock mass	3.70~4.08	507~586	−19.63~-18.29
Jintan rock mass (Tao et al., 2020)	2.86~3.69	629~691	−18.30~-17.02
Yangtze River rock mass (Zhang et al., 2017b)	3.61~4.41	599~653	−19.23~-18.44
Douzhashan rock mass (Hu et al., 2014; Pei, 2022)	2.23~5.00	576~696	−19.23~-17.89
Longyuanba rock mass (Zhong et al., 2017)	0.84~1.96	652~704	−18.62~-17.94
Fucheng rock mass (Zhao et al., 2016b; Gao, 2016)	2.95~5.91	499~697	−18.84~-17.74
Zhuguangshan rock mass (Gao et al., 2014; Zhang et al., 2011)	1.50~4.16	585~673	−19.67~-18.27
Dafushan rock mass (Zhang et al., 2011)	Average 4.95	Average 596	Average −19.07
Xiazhuang rock mass (Chen et al., 2010; Gao, 2016)	2.65~2.87	565~660	−19.59~-17.95

The pressure value is estimated based on the cited probe data; Temperature (T), pressure (P), and oxygen fugacity ($\log_{fO2}$) are estimated in Section 4.2.

that U-bearing granites in South China exhibit a wide range of temperature, pressure, and oxygen fugacity, but the ranges for each pluton are relatively concentrated. Overall, the temperature, pressure, and oxygen fugacity of the Motianling pluton are consistent with the ranges in U-bearing granites in South China. Furthermore, they closely resemble the characteristics of the Fucheng pluton in terms of temperature, pressure, and oxygen fugacity, aligning with the low-temperature and low-oxygen fugacity features typical of U-bearing granites.

The crystallization temperature of the coarse-grained granite in the Motianling pluton ranges from 501°C to 661°C, pressure ranges from 2.84 to 3.32 kbar, and oxygen fugacity ranges from −18.91 to −16.38. On the other hand, the crystallization temperature of the medium-grained granite ranges from 507°C to 586°C, pressure ranges from 3.70 to 4.08 kbar, and oxygen fugacity ranges from −19.63 to −18.29. The characteristics of the medium-grained granite are more consistent with the typical temperature, pressure, and oxygen fugacity features observed in most South China U-bearing granite formations.

5.5 Enlightenment on U enrichment in granite

Research has determined that Motianling granite is classified as an S-type granite, resulting from partial mudstone melting (Li, 1999; Wang et al., 2006; Fang et al., 2012; Song et al., 2015). Argillaceous rocks are known to contain high levels of organic matter, which under reduced conditions, the organic matter and clay minerals within mudstone often absorb substantial amounts of uranium, illustrating uranium-rich characteristics (Zhao K. D. et al., 2016). This indicates that the Motianling granite has conditions conducive to U enrichment. Partial melting of metapelitic rocks.

After organizing the geochemical data of the two types of granites from the Motianling pluton (Table 4) (Fang et al. 2012, Xu et al., 2019). The U content in the coarse-grained granite ranges from 4.84×10^{-6} to 58.20×10^{-6} (average 19.57×10^{-6}), with a Th/U ratio ranging from 0.25 to 2.52 (average 1.69); the U content in the medium-grained granite ranges from 5.37×10^{-6} to 127.00×10^{-6} (average 36.85×10^{-6}), with a Th/U ratio ranging from 0.09 to 2.53 (average 1.08). U-enriched granites are often considered the primary source of uranium for the formation of granite-type uranium deposits (Bonnetti et al., 2018). The U content in both types of granite is several to tens of times higher than the average U content in the upper continental crust worldwide (2.8×10^{-6}), suggesting that these granites have the potential to serve as uranium source rocks for uranium deposits. The Th/U ratio plays a crucial role in determining which U-bearing accessory minerals crystallize from the magma (Cuney, 2014). High U content and low Th/U ratios favor the crystallization of crystalline uranium minerals, which are considered a potential source of uranium in granite-type uranium deposits (Hu et al., 2012). The medium-grained granite of the Motianling pluton has higher U content and lower Th/U ratios compared to the coarse-grained granite (Figure 10), indicating that the medium-grained granite has greater potential as a uranium source than the coarse-grained granite.

The oxygen fugacity during magma crystallization in Motianling granite falls below the Fe_3O_4-Fe_2O_3 (HM) buffer line (Figure 9). Under such conditions, uranium mainly exists in the form of U^{4+}. In an F-rich system, U^{4+} tends to combine with F to form complexes that migrate and enrich in the magma system (Chen et al., 2010). In the later stages of magma evolution, U^{4+} mostly combines with lithophile elements to form U-rich minerals (Ling, 2011; Hu et al., 2014). Under relatively low-temperature (<1,000°C) conditions, the solubility of U^{4+} in magma is lower, making it easier to precipitate.

(Hazen et al., 2009). Because U^{4+} has ionic radii and electronegativity similar to those of Th^{4+}, REE^{3+}, Zr^{4+}, Ce^{4+}, and Ca^{2+}, during magmatic differentiation—where uranium, being highly incompatible, is continuously enriched in the residual melt—it is incorporated into accessory minerals such as monazite,

TABLE 4 Th and U characteristics of granites in the Motianling rock mass.

Sample	Lithology	Th	U	Th/U
M029-1	Coarse-grained granite	12.20	4.84	2.52
M029-4	Coarse-grained granite	15.60	8.57	1.82
M038-1	Coarse-grained granite	14.40	6.68	2.16
Zk2-7	Coarse-grained granite	14.40	58.20	0.25
M044	Medium coarse-grained granite	12.60	6.36	1.98
M041	Medium coarse-grained granite	13.60	5.37	2.53
M078-6	Medium coarse-grained granite	12.80	77.60	0.16
M078-7	Medium coarse-grained granite	11.20	16.40	0.68
M078-1	Medium coarse-grained granite	12.90	10.00	1.29
M078-5	Medium coarse-grained granite	11.70	127.00	0.09
ZK1-5	Medium-grained granite	12.40	15.20	0.82

Data for samples M029–1, M044, M041, M078–6, M078–7, M078–1, M078-5, and ZK1-5 are from reference (Xv et al., 2019), while data for samples M029–4, M038-1, and ZK2-7 are from reference (Fang et al., 2012).

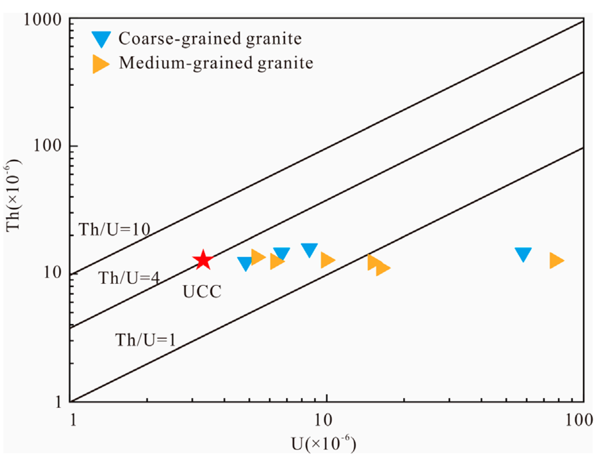

FIGURE 10
Th-U content relationship diagram.

allanite, xenotime, zircon, and apatite via isomorphic substitution (Zhang, 1990; Cuney, 2014). The remaining U combines with free oxygen O^{2-}, resulting in the formation of uraninite. Previous research has shown that granites may act as a possible source of U in granite-type U deposits (Hu et al., 2012). An environment with low oxygen fugacity, corresponding to relatively reducing conditions, is conducive to the preservation of U-rich minerals. Furthermore, studies have shown that uranium migration occurs at relatively high temperatures (Hazen et al., 2009). The cooling of magma facilitates the retention of uranium in granite, thereby providing an ample uranium source for subsequent mineralization (Wang et al., 2022).

Coarse-grained granite, as a product of the early phase of late stage magmatic evolution, may be significantly influenced by source-rocks characteristics. The U enrichment observed in coarse-grained granite likely reflects the contribution of U adsorption by argillaceous rocks within the source area. In contrast, medium-grained granite, which crystallizes at a late phase of late stage magmatic, exhibits higher U content than coarse-grained granite. This suggests that relatively low oxygen fugacity and elevated concentrations of the volatile component F play a crucial role in U enrichment during the later stages of magmatic evolution. These findings underscore the indicative significance of biotite's geochemical characteristics in evaluating the U enrichment potential of granites.

Based on the discussion above, the Motianling granite exhibits favorable source and physical conditions for U enrichment. However, the overall low F content in biotite within the Motianling granite may affect U migration and enrichment, and it may also suggest that U complexes are not the primary mechanism for U enrichment in the.

Motianling pluton. Within the Motianling pluton, the medium-grained granite, compared to the coarse-grained granite, demonstrates higher U content, lower Th/U ratios, lower crystallization temperatures and oxygen fugacity, and higher F content. This implies that the medium-grained granite in Motianling pluton is more likely to enrich U.

6 Conclusion

By conducting geochemical analysis and in-depth discussion of biotite in the Motianling pluton, we have obtained the following insights.

(1) In the Motianling coarse-grained granite, biotite is predominantly Fe-biotite, while in the medium-grained granite, it is predominantly siderophyllite. Genetically, biotite in both the coarse- and medium-grained granites of the Motianling pluton is classified as magmatic biotite. Chemically, the biotite in the medium-grained granite exhibits relatively higher Al and Fe content but lower Mg and Ti content compared to that in the coarse-grained granite.
(2) The geochemical characteristics of biotite indicate that the Motianling granite belongs to the peraluminous suite, with granite originating from a crustal source. The crystallization environment is characterized by low oxygen fugacity and low crystallization temperatures, which provides indicative meaning into the U enrichment potential of the granite.
(3) Biotite in the medium-grained granite of Motianling pluton exhibits higher U content, lower Th/U ratios, lower temperature and lower oxygen fugacity compared to biotite in the coarse-grained granite. This indicates that the medium-grained granite is more conducive to U enrichment, suggesting a higher U mineralization potential.

Data availability statement

The original contributions presented in the study are included in the article/supplementary material, further inquiries can be directed to the corresponding authors.

Author contributions

PL: Writing – original draft. CG: Conceptualization, Writing – review and editing. QP: Writing – review and editing. NW: Writing – review and editing. NL: Writing – review and editing.

Funding

The author(s) declare that no financial support was received for the research and/or publication of this article.

Acknowledgments

We thank Prof. Huan Li for his efficient editorial processing. Two reviewers are also thanked for their careful reviews that resulted in an improved manuscript. We thank Dr. Yuhang Zheng and Dr. Dongren Li from the China University of Geosciences for their advisory contributions and technical assistance during the manuscript revision process.

Conflict of interest

Authors CG and NL were employed by China National Nuclear Corporation (CNNC) Beijing Research Institute of Uranium Geology and China National Nuclear Corporation (CNNC) Key Laboratory of Uranium Resource Exploration and Evaluation Technology.

The remaining authors declare that the research was conducted in the absence of any commercial or financial relationships that could be construed as a potential conflict of interest.

Generative AI statement

The author(s) declare that no Generative AI was used in the creation of this manuscript.

Publisher's note

References

Abdel, F. M., and Abdel, R. (1994). Nature of biotites from alkaline, calc-alkaline, and peraluminous magmas. *J ournal Petrology* 35, 525–541. doi:10.1093/petrology/35.2.525

Azadbakht, Z., Lentz, D., and McFarlane, C. (2017). *Geochemical characteristics of magmatic mica as a monitor of metal fertility in Devonian intrusions of the New Brunswick Appalachians Canada. SGA Program*. Fredericton, NB, Canada: University of New Brunswick, 1065–1069. Available online at: https://www.researchgate.net/publication/319433832.

Azadbakht, Z., Lentz, D. R., McFarlane, C. R. M., and Whalen, J. B. (2020). Using magmatic biotite chemistry to differentiate barren and mineralized Silurian–Devonian granitoids of New Brunswick, Canada. *Contributions Min eralogy Petrology* 175, 69. doi:10.1007/s00410-020-01703-2

Beane, R. E. (1974). Biotite stability in the porphyry copper environment. *Econ. Geol.* 69, 241–256. doi:10.2113/gsecongeo.69.2.241

Bonnetti, C., Liu, X. D., Mercadier, J., Cuney, M., Deloule, E., Villeneuve, J., et al. (2018). The genesis of gra nite-related hydrothermal uranium deposits in the Xiazhuang and Zhuguang ore fields, North Guangdong Province, S E China: insights from mineralogical, trace elements and U-Pb isotopes signatures of the U mineralisation. *Ore Geol. ogy Rev.* 92, 588–612. doi:10.1016/j.oregeorev.2017.12.010

Buddington, A. F., and Lindsley, D. (1964). Iron-titanium oxide minerals and synthetic equivalents. *J. pe trology* 5, 310–357. doi:10.1093/petrology/5.2.310

Burkhard, D. J. (1991). Temperature and redox path of biotite-bearing intrusives: a method of estimation applied to S-and I-type granites from Australia. *Earth Planet. Sci. Lett.*, 104, 89–98. doi:10.1016/0012-821x(91)90240-i

Chen, F. L., Wang, J., Cui, X. Z., Lin, S. F., Ren, G. M., Deng, Q., et al. (2024a). A latest Mesoproterozoic a rc–back-arc system in the southwestern Yangtze Block, South China: implications for paleogeographic configuration o f the Rodinia supercontinent. *Precambrian Res.* 409, 107432. doi:10.1016/j.precamres.2024.107432

Chen, X., Wen, C. H., Huang, L. Q., Li, B., and Zeng, G. Q. (2024b). Constraints on the rare-metal mineralisat ion by the *in-situ* geochemical compositions of biotites in intrusions in the Mufushan area, NE Hunan. *Acta Mineral. Sin.* 44, 1–17. doi:10.3724/j.1000-4734.2024.44.078

Chen, Y. W., Bi, X. W., Hu, R. Z., and Dong, S. H. (2012). Element geochemistry, mineralogy, geochronology and zircon Hf isotope of the Luxi and Xiazhuang granites in Guangdong province, China: implications for U mineral ization. *Lithos* 150, 119–134. doi:10.1016/j.lithos.2012.06.025

Chen, Y. W., Bi, X. W., Hu, R. Z., Zhu, W. G., Xu, L. L., and Dong, S. H. (2010). The geochemical characte ristics of biotites and their constraints on uranium mineralization in guidong pluton. *Bull. Mineralogy, Petrol ogy Geochem.*, 29, 355–363.

Cuney, M. (2014). Felsic magmatism and uranium deposits. *Bull. Société Géologique Fr.* 185, 75–92. doi:10.2113/gssgfbull.185.2.75

Czamanske, G. K., Ishihara, S., and Atkin, S. A. (1981). Chemistry of rock-forming minerals of the CretaceousPaleocene batholith in southwestern Japan and implications for magma genesis. *J. Geophys. Res. Soli d Earth* 86, 10431–10469. doi:10.1029/JB086iB11p10431

David, R. W., and Hans, P. E. (1965). Stability of biotite: experiment, theory, and application1. *Am. Minera logist* 50, 1228–1272.

Fang, Y. K., Xu, Z. Q., Tang, C. Y., Cheng, F. G., Liang, J., Qi, J. M., et al. (2012). Geological and geochem ical characteristics of granite in motianling, north guangxi province. *Guangdong Weiliang Yuansu Kexue* 19, 50–59. doi:10.16755/j.cnki.issn.1006-446x.2012.07.001

Foster, M. D. (1960). Interpretation of the composition of trioctahedral micas. *U. S. Geol. Surv. Prof. Pap.*, 1–49. doi:10.3133/pp354B

Gao, F., Pang, Y. Q., Lin, J. R., and Hu, Z. H. (2014). Mineral composition of biotites in granites of the zhu guang-mianhuakeng uranium deposit and its petrogenetic and metallogenic significance. *Bull. Mineralogy, Petr ology Geochem.* 33, 384–388. doi:10.3969/j.issn.1007-2802.2014.03.013

Gao, P. (2016). *A geochemical study of mesozoic granites from the nanling range in SouthSouth China [doctor's thesis]*. University of Science and Technology of China, Hefei, China

Hazen, R. M., Ewing, R. C., and Sverjensky, D. A. (2009). Evolution of uranium and thorium minerals. *Americ Mineralogist* 94, 1293–1311. doi:10.2138/am.2009.3208

Henry, D. J., Guidotti, C. V., and Thomson, J. A. (2005). The Ti-saturation surface for low-to-medium pressure metapelitic biotites: implications for geothermometry and Ti-substitution mechanisms. *Am. mineralogist* 90, 316328. doi:10.2138/am.2005.1498

Hu, H., Wang, R. C., Chen, W. F., Ding, H. H., Chen, P. R., and Ling, H. F. (2012). Study on uranium resou rce minerals of douzhashan uranium-bearing Granite,Northeastern guangxi. *Geol. Rev.*, 58, 1056–1068. doi:10.16509/j.georeview.2012.06.002

Hu, H., Wang, R. C., Chen, W. F., Ding, H. H., Ling, H. F., Chen, P. R., et al. (2014). Characteristics of Bioti te in Uranium- and Non-uranium-bearing Granites from Northeastern Guangxi Province, China: Implications on Urani um Mineralization. *Acta Mineral. Sin.* 34, 321–327. doi:10.16461/j.cnki.1000-4734.2014.03.004

Jacobs, D. C., and Parry, W. T. (1976). A comparison of the geochemistry of biotite from some basin and range stocks. *Econ. Geol.* 71, 1029–1035. doi:10.2113/gsecongeo.71.6.1029

Kong, H., Li, H., Wu, Q. H., Xi, X. S., Dick, J. M., and Gabo-Ratio, J. A. S. (2018). Co-development of Juras sic I-type and A-type granites in southern Hunan, South China: Dual control by plate subduction and intraplate mant le upwelling. *Geochemistry* 78, 500–520. doi:10.1016/j.chemer.2018.08.002

Li, H., Palinkaš, L. A., Watanabe, K., and Xi, X. S. (2018). Petrogenesis of Jurassic A-type granites associated with Cu-Mo and W-Sn deposits in the central Nanling region, South China: relation to mantle upwelling and intra-c ontinental extension. *Ore Geol. Rev.* 92, 449–462. doi:10.1016/j.oregeorev.2017.11.029

Li, H., Zhou, J. Q., Ouyang, L. M., Algeo, T. J., Sun, W. B., Xie, Y. M., et al. (2024). Multi-stage magmatism and Sn-polymetallic mineralization in the shuicheng region, SW China. *Lithos* 478-479, 107624. doi:10.1016/j.lithos.2024.107624

Li, J., Zou, M. L., Liu, Z. J., Zhang, T., and Zhang, J. (2021). The geochemical characteristics and accessory minerals of biotite from U deposit bearing and U deposit barren granite in douzhashan area. *Uranium Geol.* 37, 1–14. doi:10.3969/j.issn.1000-0658.2021.37.003

Li, X. H. (1999). U-Pb zircon ages of granites from northern Guangxi and their tectonic significance. *Geochimi ca*, 1–9. doi:10.19700/j.0379-1726.1999.01.001

Lin, W. W., and Peng, L. J. (1994). *The estimation of Fe3+ and Fe2+ contents in amphibole and biotite from E MPA data*. Journal of Changchun University of earth sciences, 155–162. doi:10.13278/j.cnki.jjuese.1994.02.005

Ling, H. F. (2011). Origin of hydrothermal fluids of granite-type uranium deposits: constraints from RedoxConditions. *Geol. Rev.* 57, 193–206. doi:10.16509/j.georeview.2011.02.001

Liu, B., Ma, C. Q., Liu, Y. Y., and Xiong, F. H. (2010). Mineral chemistry of biotites from the Tongshankou C u- Mo deposit: implications for petrogenesis and mineralization. *Acta Petrologica Mineralogica*, 29, 151–165.

Liu, C. S. (1984). Comparison of chemical composition of biotite minerals in granites of different origins in So uth China. *J. Guilin Inst. Metallurgical Geol.*, 1–14.

Madayipu, N., Li, H., Ghaderi, M., Soh Tamehe, L., Zhou, H. X., Wu, Q. H., et al. (2023). Contrasting Nb-Ta mineralization between the Mufushan and Lianyunshan granites, South China: evidence from whole-rock and zircon geochemistry and geochronology. *Ore Geol. Rev.* 158, 105487. doi:10.1016/j.oregeorev.2023.105487

Maydagán, L., Franchini, M., Impiccini, A., and Lentz, D. (2016). Phyllosilicates geochemistry and distribution i n the Altar porphyry Cu-(Au) deposit, Andes Cordillera of San Juan, Argentina: applications in exploration, geother mometry, and geometallurgy. *J. Geochem. Explor.* 167, 83–109. doi:10.1016/j.gexplo.2016.05.002

Meng, C. L., Bai, L. A., Yue, Z. H., Zhou, S. Y., Dai, Y., Feng, Z. H., et al. (2024). Fluid inclusion characteri stics and mechanisms of tin mineralisation in the Jialong tin polymetallic deposits, Jiuwandashan–Yuanbaoshan, northe rn Guangxi, China. *Aust. J. Earth Sci.* 71, 988–1004. doi:10.1080/08120099.2024.2427093

Pei, L. N. (2022). *Study on zircon mineral inclusions and geochemistry of uranium rich granite [master's thesis]*. Beijing Geological Research Institute of Nuclear Industry, Beijing, China

Qiu, L., Yan, D. P., Ren, M. H., Cao, W. T., Tang, S. L., Guo, Q. Y., et al. (2018). The source of uranium wi thin hydrothermal uranium deposits of the Motianling mining district, Guangxi, South China. *Ore Geol. Rev.* 96, 201–217. doi:10.1016/j.oregeorev.2018.04.001

Qiu, L., Yan, D. P., Tang, S. L., Arndt, N. T., Fan, L. T., Guo, Q. Y., et al. (2015). Cooling and exhumation of the oldest Sanqiliu uranium ore system in Motianling district, South China Block. *Terra nova*, 27, 449–457. doi:10.1111/ter.12179

Qiu, L., Yan, D. P., Tang, S. L., Chen, F., Song, Z. D., Gao, T., et al. (2020). Insights into post-orogenic exten sion and opening of the Palaeo-Tethys Ocean recorded by an Early Devonian core complex in South China. *J. Geodyn.* 135, 101708. doi:10.1016/j.jog.2020.101708

Rasmussen, K. L., and Mortensen, J. K. (2013). Magmatic petrogenesis and the evolution of (F:Cl:OH) fluid composition in barren and tungsten skarn-associated plutons using apatite and biotite compositions: case studies from the northern Canadian Cordillera. *Ore Geol. Rev.* 50, 118–142. doi:10.1016/j.oregeorev.2012.09.006

Sarjoughian, F., Kananian, A., Ahmadian, J., and Murata, M. (2015). Chemical composition of biotite from the Kuh-e Dom pluton, Central Iran: implication for granitoid magmatism and related Cu–Au mineralization. *Arabian Jou rnal Geosciences* 8, 1521–1533. doi:10.1007/s12517-013-1242-5

Selby, D., and Nesbitt, B. E. (2000). Chemical composition of biotite from the Casino porphyry Cu–Au–Mo min eralization, Yukon, Canada: evaluation of magmatic and hydrothermal fluid chemistry. *Chem. Geol.* 171, 77–93. doi:10.1016/S0009-2541(00)00248-5

Shu, L. S., Yao, J. L., Wang, B., Faure, M., Charvet, J., and Chen, Y. (2021). Neoproterozoic plate tectonic pro cess and Phanerozoic geodynamic evolution of the South China Block. *Earth-Science Rev.* 216, 103596. doi:10.1016/j.earscirev.2021.103596

Song, H., Xu, Z. Q., Ni, S. J., Zhang, C. J., Liang, J., Cheng, F. G., et al. (2015). Response of the motianling granitic pluton in north guangxi to the tectonic evolution in the southwestern section of the jiangnan orogenic belt: constraints from neoproterozoic zircon geochronology. *Geotect. Metallogenia* 39, 1156–1175. doi:10.16539/j.ddgzyckx.2015.06.015

Stone, D. (2000). Temperature and pressure variations in suites of Archean felsic plutonic rocks, Berens River a rea, northwest Superior Province, Ontario, Canada. *Can. Mineralogist*, 38, 455–470. doi:10.2113/gscanmin.38.2.455

Taghavi, A., Maanijou, M., Lentz, D. R., Sepahi-Gerow, A. A., Maruoka, T., Fujisaki, W., et al. (2022). Biotite compositions and geochemistry of porphyry-related systems from the central Urumieh Dokhtar Magmatic Belt, wester n Yazd, Iran: insights into mineralization potential. *Lithos*, 412-413, 106593. doi:10.1016/j.lithos.2022.106593

Tang, P., Chen, Y. C., Tang, J. X., Wang, Y., Zheng, W. B., Leng, Q. F., et al. (2019). Advances in research of mineral chemistry of magmatic and hydrothermal biotites. *Acta Geol. Sin. - Engl. Ed.* 93, 1947–1966. doi:10.1111/1755-6724.14395

Tang, P., Tang, J. X., Zheng, W. B., Leng, Q. F., and Lin, B. (2017). Progress in study of mineral chemistry of magmatic and hydrothermal biotites. *Mineral. Deposits* 36, 935–950. doi:10.16111/j.0258-7106.2017.04.010

Tao, J. H., Lin, Q. L., Li, X. H., Cao, J., Wang, A. D., and Xv, Z. T. (2020). Mineral chemical characteristics of biotites from the jintan granites in jiangxi province and the implication for uranium enrichment. *Bull. Mi neralogy, Petrology Geochem.* 39, 267–282. doi:10.19658/j.issn.1007-2802.2019.38.125

Uchida, E., Endo, S., and Makino, M. (2007). Relationship between solidification depth of granitic rocks and for mation of hydrothermal ore deposits. *Resour. Geol.* 57, 47–56. doi:10.1111/j.1751-3928.2006.00004.x

Wan, K., Liu, L., Meng, P. H., and Xia, Y. C. (2022). Review of the biotite mineral chemical characteristics of uranium-bearing and uranium-barren granite plutons in south China. *Mineral. Explor.* 13, 1241–1249. doi:10.20008/j.kckc.202209001

Wang, D. Z., Leng, C. B., Qin, C. J., Duan, F. H., Zhou, W. P., and Xu, D. R. (2022). Geochemical characteri stics and mineralization of uranium. *Geotecht. Metallogenia*, 46, 282–302. doi:10.16539/j.ddgzyckx.2022.02.007

Wang, X. L., Zhou, J. C., Qiu, J. S., Zhang, W. L., Liu, X. M., and Zhang, G. L. (2006). Petrogenesis of the Neoproterozoic strongly peraluminous granitoids from Northern Guangxi: constraints from zircon geochronology and Hf isotopes. *Acta Petrol. Sin.*, 22, 326–342.

Wang, Y. J., Pang, Y. Q., Fan, H. H., Zhang, J., and Ma, Q. K. (2024a). *In-situ* geochronology and geochemist ry of pitchblende from Xincun uranium deposit in motianling area. *North Guangxi Earth Sci.* 49, 1307–1323. doi:10.3799/dqkx.2022.467

Wang, Y. J., Shu, L. S., Zhang, Y. Z., Cawood, P. A., Qian, X., Gan, C. S., et al. (2024b). Proterozoic tectonic s of eastern South China and their Paleo-location reconstruction. *ACTA Sci. Nat. UNIVERSI TATIS SUNYATSENI* 63, 1–25. doi:10.13471/j.cnki.acta.snus.ZR20240043

Wang, Z. Y., Chen, Y. R., and Liu, Y. Z. (2020). Comparison of geochemical characteristics of granite rocks ma ss in Northwest Guangxi and its geological implication. *Mineral Resour. Geol.* 34, 752–760. doi:10.19856/j.cnki.issn.1001-5663.2020.04.014

Xu, Z. Q., Song, H., Yin, M. H., Zhang, C. J., Cheng, F. G., and Tang, C. Y. (2019). Uranium metallogenic m echanism of Neoproterozoic granites in South China: a case study from the Motianling granite. *Acta Pet. Sin.* 35, 2695–2710. doi:10.18654/1000-0569/2019.09.05

Yao, J. L., Cawood, P. A., Shu, L. S., and Zhao, G. C. (2019). Jiangnan orogen, South China: a ~970–820 MaRodinia margin accretionary belt. *Earth-Science Rev.* 196, 102872. doi:10.1016/j.earscirev.2019.05.0166

Yin, R., Li, H., Huang, X. L., Li, J., Li, W. X., and Chen, L. L. (2019). Textural and chemical variations of m icas as indicators for tungsten mineralization: evidence from highly evolved granites in the Dahutang tungsten deposi t, *South China*. 104, 949–965. doi:10.2138/am-2019-6796

Zhang, C. J. (1990). The features of uraninite in guidong granite complex and its significance to search for ura nium deposit. *J. Chengdu Inst. Geosciences*, 10–17+131.

Zhang, G. W., Guo, A. L., Wang, Y. J., Li, S. Z., Dong, Y. P., Liu, S. F., et al. (2013). Tectonics of South Ch ina continent and its implications. *Sci. China Earth Sci.* 56, 1804–1828. doi:10.1007/s11430-013-4679-1

Zhang, J., Chen, W. F., and Chen, P. R. (2011). Compositional differences of the biotites from the uranium-for ming and non uranium-forming indosinian granites in SouthSouth China. *Geotecht. Metallogenia* 35, 270–277. do i. doi:10.16539/j.ddgzyckx.2011.02.010

Zhang, L., Chen, Z. Y., Li, S. R., Santosh, M., Huang, G. L., and Tian, Z. J. (2017a). Isotope geochronology, geochemistry, and mineral chemistry of the U-bearing and barren granites from the Zhuguangshan complex, South China: implications for petrogenesis and uranium mineralization. *Ore Geol. Rev.* 91, 1040–1065. doi:10.1016/j.oregeorev.2017.07.017

Zhang, L., Chen, Z. Y., Tian, Z. J., Huang, G. L., and Tian, X. L. (2017b). Chemical composition of biotite an d chlorite in the uranium-bearing and barren granites,northern Guangdong Province,South China: implications for uran ium mineralization. *Earth Sci. Front.* 24, 62–75. doi:10.13745/j.esf.yx.2017-1-7

Zhang, L., Chen, Z. Y., Wang, F. Y., and Zhou, T. F. (2021). Whole-rock and biotite geochemistry of granites fr om the Miao'ershan batholith, South China: implications for the sources of granite-hosted uranium ores. *Ore Geol. Rev.* 129, 103930. doi:10.1016/j.oregeorev.2020.103930

Zhang, W. C., Zhao, Z. D., Liu, D., Qiu, K. F., Wang, Q., Zhu, D. C., et al. (2023). Mineralogy and geochemi stry of the Zedong Late Cretaceous (94 Ma) biotite granodiorite in the Southern Lhasa Terrane: Implications for th e tectonic setting and Cu-Au mineralization. *Lithos* 446-447, 107158. doi:10.1016/j.lithos.2023.107158

Zhao, J. H., Zhou, M. F., and Zheng, J. P. (2013). Constraints from zircon U–Pb ages, O and Hf isotopic comp ositions on the origin of Neoproterozoic peraluminous granitoids from the Jiangnan Fold Belt, South China. *Contribut ions Mineralogy Petrology* 166, 1505–1519. doi:10.1007/s00410-013-0940-z

Zhao, K. D., Jiang, S. Y., Ling, H. F., Sun, T., Chen, W. F., Chen, P. R., et al. (2016a). Late Triassic U-bearin g and barren granites in the Miao'ershan batholith, South China: petrogenetic discrimination and exploration significa nce. *Ore Geol. Rev.* 77, 260–278. doi:10.1016/j.oregeorev.2016.02.016

Zhao, L. Z., Liu, C. S., and Sun, N. (1983). *The Petrological characteristics of the Taiping-Huangshan polygenet ic composite batholith in southern Anhui.* Journal of Nanjing University (Natural Science Edition), 329–391.

Zhao, Y. D., Wu, J. Q., Ling, H. F., and Wang, H. Z. (2016b). Mineral chemistry of biotite and chlorite in wes tern part of Fucheng granite,southern Jiangxi Province: implications for uranium mineralization. *Mineral. Deposits* 35, 153–168. doi:10.16111/j.0258-7106.2016.01.010

Zhao, Z. B., Xu, Z. Q., Ma, X. X., Liang, F. H., and Guo, P. (2018). Neoproterozoic–early paleozoic tectonic evolution of the SouthSouth China craton: new insights from the polyphase deformation in the southwestern jiangnan O rogen. *Acta Geol. Sin. - Engl. Ed.* 92, 1700–1727. doi:10.1111/1755-6724.13672

Zhong, F. J., Pan, J. Y., Xu, Y., Qi, J. M., Shu, T. T., Mou, P., et al. (2017). Mineral chemistry of biotites an d chlorites from huangsha uranium mining area in the Middle nangling range: constraints on petrogenesis and U ranium mineralization. *Geol. J. China Univ.* 23, 575–590. doi:10.16108/j.issn1006-7493.2017015

Zhou, Z. X. (1986). The origin of intrusive mass in fengshandong, Hubei province. *Acta Petrol. Ainica*, 5970.